Journal of Sound and Vibration (1999) **220**(1), 27–65
Article No. jsvi.1998.1915, available online at http://www.idealibrary.com on IDEAL

NON-LINEAR STOCHASTIC DYNAMICS OF TENSION LEG PLATFORMS

R. ADREZIN

Department of Mechanical Engineering, *University of Hartford*, *West Hartford*, *CT* 06117-1599, *U.S.A.*

AND

H. BENAROYA

Department of Mechanical and Aerospace Engineering, *Rutgers University*, *Piscataway*, *NJ* 08855-0909, *U.S.A.*

(*Received* 20 *January* 1998, *and in final form* 28 *July* 1998)

In this paper, a set of non-linear equations of motion for a single-tendon tension leg platform are developed. The equations of motion consist of partial differential equations representing the transverse and longitudinal response of the tendon. In addition, a mixed formulation partial differential equation describing the surge response of the hull and tendon, coupled with an ordinary differential equation for the pitch response of the rigid hull is presented. Many of the simplifying assumptions used by prior researchers have been eliminated. The hull is modelled as a hollow rigid cylindrical body, and the tendon as a hollow cylindrical beam pinned at its top to the hull and at its bottom to the template connected to the seafloor. The Extended Hamilton's Principle is applied and the Lagrangian is fully developed. Terms include the kinetic energy, bending and membrane strain energies and the potential energy due to gravity and buoyancy. The normalized equations of motion are also detailed. The full derivation with assumptions are presented. The response, analyzed for stochastic wave and current loading, is presented with a planar motion assumption. The tension leg platform will oscillate about its vertical position due to ocean waves. Current will cause a tension leg platform to oscillate about an offset position rather than its vertical position. This offset in the surge direction has a corresponding setdown, the lowering of the hull in the heave direction, which increases the buoyancy forces. This results in a higher tension in the tendons than if the tendon and hull were in a vertical position. Forces on the tendon have been neglected in much of the literature. The responses presented in this work show that the inclusion of forces on the tendon will result in both a greater amplitude and offset position when compared to studies where these forces are neglected. This offset position, which is the surge displacement from the vertical position, is significant in the operation of a tension leg platform. A Monte Carlo simulation was performed on the drag and inertia coefficients in Morison's equation. A uniform random distribution of coefficients was selected from 0·6 to 2·0 for each coefficient. Twenty computer simulations were implemented for each coefficient. The response showed that the offset position and the amplitude are both dependent on the drag coefficient. The surge of the hull shows a maximum offset approximately three times greater for the coefficient that

0022–460X/99/060027 + 39 $30.00/0

resulted in the maximum displacement than the minimum. The response did not show a significant dependence on the inertia coefficient, however, this is not necessarily true for unsteady current, large hull and tendon diameters, ocean wave frequencies greater than 1 rad/s, and low current velocity.

1. INTRODUCTION

The Tension Leg Platform (TLP) is an offshore structure particularly well suited for deep-water operation. Unlike fixed structures, the cost of a compliant TLP does not dramatically increase with water depth. The TLP is vertically moored at each corner of the hull minimizing the heave, pitch and roll of the platform. This small vertical motion results in less expensive production equipment than would be required on a semisubmersible [1, 2].

TLPs are complete oil and natural gas production facilities costing US $1 billion or more [3]. The supporting structure of a TLP consists of a hull, tendons and templates, as shown in Figure 1. The hull is a buoyant structure with a deck at its top that supports the oil production facility and crew housing. Pontoons and columns provide sufficient buoyancy to maintain the deck above the waves during

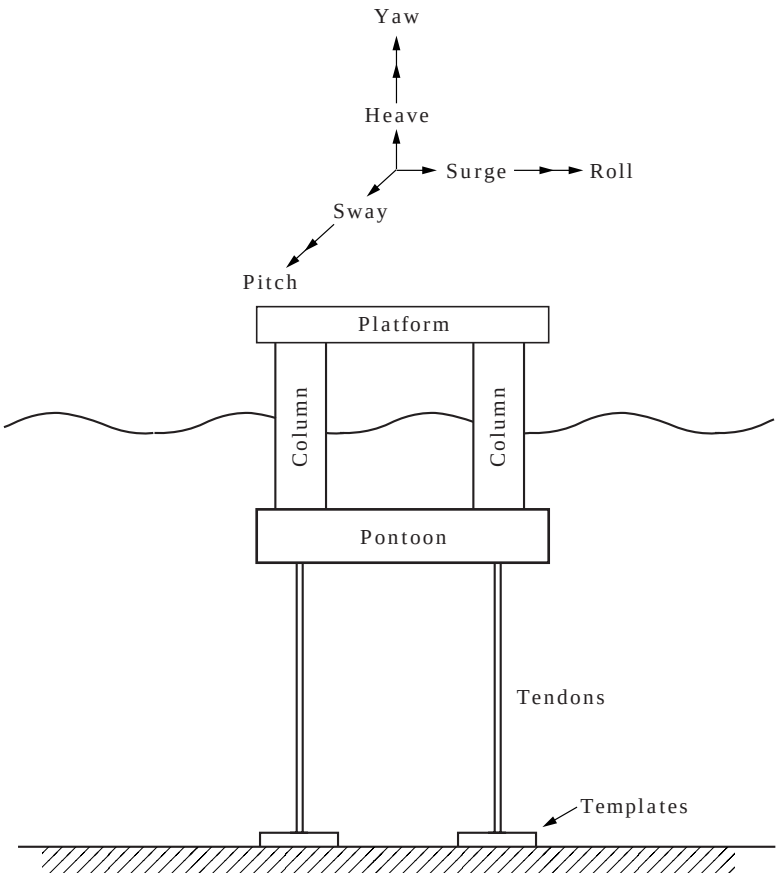

Figure 1. Schematic of a tension leg platform.

all sea states. These columns are moored to the seafloor through tendons, and fixed in place with templates. The hull's buoyancy creates tension in the tendons.

The tallest TLP at the time of its construction, Shell Oil's Auger TLP in the Gulf of Mexico, began production in 1994 after an investment of six years and US $1·2 billion. The Auger TLP with a crew of 112 has two main decks 90 by 90 m (300 by 300 ft) with a well bay at its center. Four cylindrical columns 22·5 m (74 ft diameter) and pontoons [8·5 × 10·7 m (28 by 35 ft) cross-section] comprise the hull. There are three tendons at each column. Each tendon also known as tether or tension leg, was assembled from 12 steel pipes with a 66-cm (26-in.) diameter and a 3·3-cm (1·3-in.) wall thickness, connected end to end, and a total length of 884 m (2900 ft). During severe storms it may surge 72 m (235 ft) [3, 4].

The surge, sway and yaw resonance frequencies of TLPs are below that of the wave frequency range as defined by a power spectrum such as the Pierson–Moskowitz. The heave, pitch and roll resonance frequencies are above this range. The resulting response is a desirable feature of TLPs. Wind, waves and current will cause a TLP to oscillate about an offset position rather than its vertical position. This offset in the surge direction has a corresponding setdown, the lowering of the TLP in the heave direction, which increases the buoyancy forces. This results in a higher tension in the tendons than if it was in the vertical position. Higher order effects due to the non-linear nature of the waves and non-linear structural properties will affect the dynamic response and may be of interest. Papers that include varying levels of higher order effects are discussed in a review paper by Adrezin *et al*. [5]. A study of the dynamics of compliant offshore structures is found in the text by Bar-Avi and Benaroya [6].

2. PROBLEM DESCRIPTION

In this paper, a set of non-linear equations of motion for a single-tendon tension leg platform is developed. Many of the simplifying assumptions used by prior researchers, such as modelling the tendon as a massless spring, have been eliminated. The response is analyzed for random wave and current loading. Planar motion is considered and the equations of motion for the tendon and the hull is coupled. The hull is modelled as a hollow rigid cylindrical body, the tendon as a hollow cylindrical beam pinned at its top to the hull and at its bottom to the template. The response is determined numerically in the time domain by implementing a finite difference scheme.

3. EXTENDED HAMILTON'S PRINCIPLE

The Extended Hamilton's Principle is a method utilizing the calculus of variations [7] for deriving the equations of motion and boundary conditions for deformable bodies [8]. The Extended Hamilton's Principle may be expressed as

$$\delta \int_{t_1}^{t_2} T \, \mathrm{d}t = -\delta \int_{t_1}^{t_2} W \, \mathrm{d}t, \tag{1}$$

where δ represents a virtual change, T is the kinetic energy and δW is the virtual work. The virtual work may be expressed as

$$\delta W = -\delta V + \delta W_{nc}, \tag{2}$$

where V is the potential energy and δW_{nc} represents the virtual work due to non-conservative forces.

In this paper, equation (1) is rewritten as

$$\delta \int_{t_1}^{t_2} \mathscr{L} \, \mathrm{d}t = -\delta \int_{t_1}^{t_2} W \, \mathrm{d}t, \tag{3}$$

where $\mathscr{L}$ is the Lagrangian, the difference between the kinetic and potential enegy,

$$\mathscr{L} = T - V, \tag{4}$$

and the expression for virtual work is

$$\delta W = \hat{Q}^v \delta v + \hat{Q}^x \delta u, \tag{5}$$

where $\hat{Q}^x$ and $\hat{Q}^y$ are the generalized forces per unit length associated with the generalized co-ordinates u and v, and δu and δv are virtual displacements.

4. ASSUMPTIONS

Several assumptions are outlined in this section. They pertain to the physical properties of a TLP and simplify the analysis. The extent and the validity are discussed below. In addition, other assumptions are presented within the body of this work preceding their application.

Tendon length is much greater than its diameter, $\ell \gg D_o$.
Shear effects in the tendon need not be included.
Planar motion of the TLP.
Hull is treated as a rigid body.
Hull pitch angle is small due to excessive buoyancy forces, therefore $\phi \ll 1$.
The top of the hull always remains above the wave elevation, $L + L_H \cos\phi > d + \eta(y, t)$.
The bottom of the hull is always submerged (otherwise unstable), $L < d + \eta(y, t)$.
Hull is represented by a hollow vertical cylinder.
Center of gravity of the hull is located at the geometrical center of the hull (other locations have been analyzed).
Water level is assumed constant and horizontal across the hull's column at a given instant of time.

Since the tendon length is considered to be much greater than its diameter, shear-deformation effects are not included since these will then be considerably less than the effects due to the bending energy. In addition, high frequency motions are not of interest in the present study since they are well above the range of

loading. These two assumptions allow for the use of Euler–Bernoulli beam theory [9].

Once again, since we are interested in resonant frequencies in the range of the environmental loading, the longitudinal frequencies may be neglected. The natural frequencies for transverse vibration are significantly lower than those for longitudinal (extensional) vibration.

The assumption of planar motion is reasonable if vortex shedding is neglected. Vortex shedding results in an out-of-plane response which needs to be explored further [10, 11].

Treatment of the hull as a rigid body is a reasonable assumption [12]. Its stiffness results in natural frequencies well above the range for wave, wind and current loading. The requirement that the top of the hull always remains above the waves is necessary to allow it to safely support oil and gas production activities. Due to the mass of the hull and the flexibility of the tendons, the bottom of the hull must always remain submerged for the system to remain stable. If not for the buoyancy forces, the tendon would buckle under its own weight.

The representation of the hull as a hollow cylinder with a center of mass located at its geometric center (along with the planar motion restriction) are the assumptions of concern. An actual hull is top heavy with the production facility and crew housing at its top and buoyant pontoons and columns at its bottom. The validity of these assumptions need to be studied further. The center of gravity can be calculated at any position by modifying equation (48), which is the vector to the center of gravity of the hull. Different locations have been tried.

The water level is assumed constant and horizontal across the hull's column at a given instant of time. This simplifies the calculation of the center of buoyancy. The validity of this assumption is dependent on the wave height, wave length, wave frequency and the column's diameter. With this assumption, the position of the center of buoyancy should be recalculated at each time step. For a typical TLP, this assumption is reasonable.

5. DERIVATION OF THE LAGRANGIAN

The Lagrangian, which is the energy functional is now derived. Applying the Extended Hamilton's Principle will result in the equations of motion and boundary conditions. The Lagrangian for the tendon, $\mathscr{L}$ is the sum of the energies:

$$\mathscr{L} = E_k - E_s - E_p, \tag{6}$$

where E_k represents the kinetic energy, E_s represents the strain energy, and E_p includes all potential energy other than strain. The Lagrangian will be expressed in terms of Eulerian co-ordinates (x, y). Applying the Extended Hamilton's Principle results in a material derivative. All velocities in this paper represent solely the local part, and not the convective part of the material derivative. This is because the convective terms are small as compared to the local terms. For systems with large motion, a Lagrangian co-ordinate system (X, Y) may be preferred.

5.1. STRAIN ENERGY

A body subject to forces may undergo rigid body motions and deformations. The rigid body motions do not allow strain and therefore do not include stress. The study of a deformable body is required to determine the strain energy of a system. Figure 2 shows an arbitrary body in its undeformed and deformed configuration. Derivations will be presented for planar motion only. A continuum mechanics text such as Fung [13] may be consulted for the derivation in three spatial dimensions. The formulation of Bottega [14] would be useful for the inclusion of base excitations (e.g., earthquakes). A point of the undeformed body has the co-ordinate (X, Y) and an attached infinitesimal line segment has the length $\mathrm{d}S$. After the body is deformed, the co-ordinates for the point (X, Y) is now (x, y) and the new length is $\mathrm{d}s$. The vertical and horizontal displacements of a point due to deformation and rigid body motion are represented by u and v, respectively. They are defined as

$$u = x - X, \qquad v = y - Y. \tag{7, 8}$$

The transverse strain e_{yy} and the shear strain e_{xy} are assumed to be substantially smaller than the axial strain e_{xx}. Therefore, only this strain will be related to displacements u and v. The axial Eulerian strain at a point in terms of the displacements is derived as

$$e_{xx} = \frac{\partial u}{\partial x} - \frac{1}{2}\left[\left(\frac{\partial u}{\partial x}\right)^2 + \left(\frac{\partial v}{\partial x}\right)^2\right]. \tag{9}$$

Assuming small strain and "moderate" rotation, $e_{xx} \ll 1$, $(\partial u/\partial x)^2 \ll \partial u/\partial x$ and $(\partial v/\partial x)^2$ is on the same order of $\partial u/\partial x$ yields

$$e_{xx} = \frac{\partial u}{\partial x} - \frac{1}{2}\left(\frac{\partial v}{\partial x}\right)^2. \tag{10}$$

The constitutive relationship where E is the modulus of elasticity is

$$\sigma = E e_{xx}. \tag{11}$$

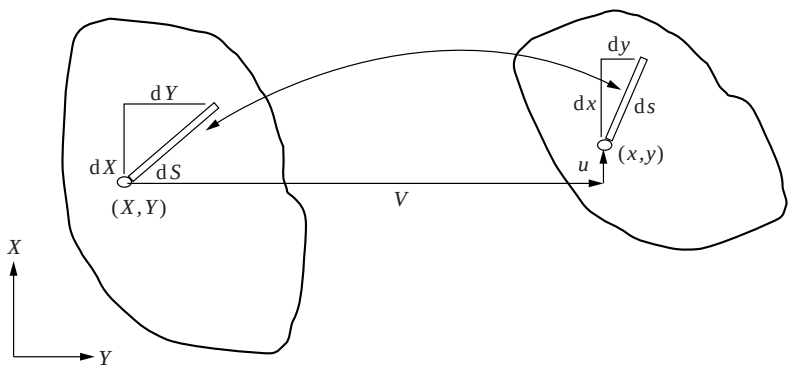

Figure 2. Undeformed body (left) and deformed body (right).

The axial strain is derived from the displacement due to membrane and bending stresses. Shear stresses will be neglected, a reasonable assumption for a long slender beam. Strain induced by torsion and temperature changes will also be neglected. This simplifies the expression and results in the bending strain energy, E_B, which may now be written as

$$E_B = \int_{s=0}^{s=\ell} \frac{1}{2} EI(s) \left(\frac{\partial \theta}{\partial s} \right)^2 \mathrm{d}s, \tag{12}$$

and a membrane strain of

$$E_M = \frac{1}{2} \int_{x=0}^{x=L} P \left[\frac{\partial u}{\partial x} - \frac{1}{2} \left(\frac{\partial v}{\partial x} \right)^2 \right] \mathrm{d}x, \tag{13}$$

where P is the tension in the tendon. An expression for the tension will be developed later in this paper. The curvaturve $\partial\theta/\partial s$ is equal to the inverse of the radius of curvature $R(x)$. This is expressed in Cartesian co-ordinates as

$$R(x) = \frac{(1 + (\partial v/\partial x)^2)^{3/2}}{\partial^2 v/\partial x^2}. \tag{14}$$

Therefore, the total strain energy is

$$E_s = E_B + E_M. \tag{15}$$

5.1.1. *Estimation of the projected tendon length L*

The vertical motion of the hull of a TLP is minimal. The following is a derivation of an estimate of the projection of the tendon length ℓ on the x-axis, referred to as L. The tendon is considered extensible, but this extension is neglected in the calculation of L. This is consistent with the small wave amplitude to water depth ratio assumption discussed subsequently.

The co-ordinate s is defined along the length of the tendon. An incremental length, $\mathrm{d}s$, is given by

$$\mathrm{d}s = \sqrt{1 + v_x(x, t)^2}\, \mathrm{d}x. \tag{16}$$

The assumption of neglecting the extension in the tendon leads to a constraint relationship between displacements u and v. Recall that $u = x - X$. From Figure 3, it can be concluded that if the beam is vertical and straight in its undeformed position, then co-ordinate $X = S$. Furthermore, if inextensible, $S = s$. This leads to the relationship $X = s$, which will be of use in developing the constraint relationship. Assigning ξ as a dummy variable for x, the co-ordinate x is defined by the relation

$$s(x) = \int_{\xi=0}^{\xi=x} \sqrt{1 + \left(\frac{\partial v(\xi, t)}{\partial \xi} \right)^2}\, \mathrm{d}\xi. \tag{17}$$

If the slope $\partial v/\partial \xi$ is assumed small ($\partial v/\partial \xi \ll 1$), which is a reasonable assumption based on the observed motion of a tension leg platform, then a binomial expansion yields the simplification

$$s = x + \frac{1}{2} v \frac{\partial v}{\partial \xi}\bigg|_{\xi=0}^{\xi=x} - \frac{1}{2} \int_{\xi=0}^{\xi=x} v \frac{\partial^2 v}{\partial \xi^2} \, \mathrm{d}\xi. \tag{18}$$

The boundary condition that $v = 0$ at the base will be applied. Solving for x and substituting into equation (7), along with $X = s$, results in the holomic constraint relationship

$$u = -\frac{1}{2} v \frac{\partial v}{\partial \xi} + \frac{1}{2} \int_{\xi=0}^{\xi=x} v \frac{\partial^2 v}{\partial \xi^2} \, \mathrm{d}\xi. \tag{19}$$

The first term accounts for the displacement and slope of the tendon. The second term accounts for the displacement and curvature of the tendon and must be solved numerically if no further assumptions are made. However, for a tension leg platform, the second term should be much smaller than the first due to the high tension in the tendons. Note that in problems where a small slope assumption is not valid, equation (17) must be evaluated numerically.

The relationship between L and ℓ is

$$L = \ell + u|_{x=L}. \tag{20}$$

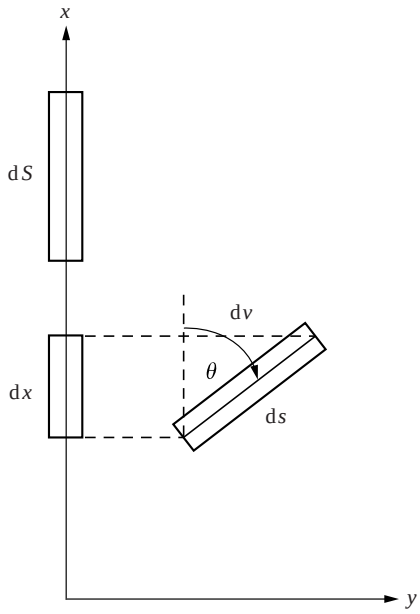

Figure 3. Incremental element of mass dm shown in its undeformed position dS, its perturbed position ds and its projection dx.

Substituting equation (19) into the above equation results in

$$L = \ell - \frac{1}{2} v \frac{\partial v}{\partial \xi}\bigg|_{\xi = L} + \frac{1}{2} \int_{\xi = 0}^{\xi = L} v \frac{\partial^2 v}{\partial \xi^2} \, \mathrm{d}\xi. \tag{21}$$

5.2. KINETIC ENERGY

The kinetic energy for the tendon will be developed next. The kinetic energy is a function of the incremental mass which is first expressed in terms of the path variable s. Ultimately, the Lagrangian will be evaluated over the spatial variable x. This requires the derivation of the incremental mass in terms of x. Relationships between the two will be presented in order to maintain a constant mass for the system.

For an incremental length of tendon in the perturbed state, $\mathrm{d}s$, the corresponding incremental mass, $\mathrm{d}\bar{m}$, is (Figure 3)

$$\mathrm{d}\bar{m} = \tfrac{1}{4}\pi[\rho_{T_p}(s)(D_o(s)^2 - D_i(s)^2) + C_A \rho_{flp}(s) D_o(s)^2] \, \mathrm{d}s. \tag{22}$$

The first term represents the mass of the tendon. The second term is the added mass [15] where C_A is the non-dimensional added mass coefficient that is related to the inertia coefficient C_M by

$$C_A = C_M - 1. \tag{23}$$

For a very large tendon length to diameter ratio, as is the case for these structures, C_M approaches its theoretical limit of 2 and C_A approaches 1. This added mass is due to the entraining of fluid particles by the motion of the tendon.

The same incremental mass expressed in equation (22) may be described as projected onto the present. Cartesian co-ordinate system's x-axis as

$$\mathrm{d}\bar{m} = \tfrac{1}{4}\pi[\rho_T(x)(D_o(x)^2 - D_i(x)^2) + C_A \rho_{fl}(x) D_o(x)^2] \, \mathrm{d}x. \tag{24}$$

If the tendon is assumed to have constant circular outer and inner diameters along the path variable s, this will result in $D_o(s) = D_o$ and $D_i(s) = D_i$.

Consider the perturbed (or present) tendon density at time t_1 and at a later time t_2, represented by $\rho_{Tp1}(s)$ and $\rho_{Tp2}(s)$, respectively. The following expression relates the densities where $\rho_{Tp1}(s)$ is multiplied by the Jacobian determinant (the determinant of the Deformation Gradient):

$$\rho_{Tp1}(s) = \det \begin{bmatrix} \dfrac{\partial x}{\partial X} & \dfrac{\partial x}{\partial Y} \\ \dfrac{\partial y}{\partial X} & \dfrac{\partial y}{\partial Y} \end{bmatrix} \rho_{Tp1}(s). \tag{25}$$

The Jacobian determinant may be expressed as

$$\det \begin{bmatrix} \dfrac{\partial x}{\partial X} & \dfrac{\partial x}{\partial Y} \\ \dfrac{\partial y}{\partial X} & \dfrac{\partial y}{\partial Y} \end{bmatrix} = 1 + O(e_{xx}^2) \approx 1, \tag{26}$$

due to small deformation, which leads to

$$\rho_{Tp2}(s) = \rho_{Tp1}(s) \approx \rho_{Tp}, \tag{27}$$

and therefore the perturbed density is assumed to be constant.

Water density will also be assumed constant: $\rho_{flp}(s) = \rho_{flp}$. When the perturbed length $\mathrm{d}s$ is projected onto the x-axis, it results in a length $\mathrm{d}x \leqslant \mathrm{d}s$ due to bending strain. (See Figure 3.) One can see that the upper bound $\mathrm{d}x = \mathrm{d}s$ occurs when the tendon is in its undeformed (vertical) position. Membrane strain, however, may cause $\mathrm{d}s > \mathrm{d}x$.

The Lagrangian will be integrated along the x-axis. The projection of the tendon length ℓ onto the x-axis, results in a projected length L which is less than or equal to ℓ. In order to maintain a constant mass, the incremental mass in the x–y frame may be written with a constant density and varying diameters to represent an elliptical horizontal cross-section of the deformed tendon. A second alternative assumes that the constant diameters along the path variable s will be used, and the density will vary. For instance, to account for $\mathrm{d}x < \mathrm{d}s$ the density will increase $\rho_T(x) > \rho_{Tp}$. Applying the second alternative with these assumptions yields the new relationship for $\mathrm{d}\bar{m}$, following equations (22) and (24):

$$\mathrm{d}\bar{m} = \tfrac{1}{4}\pi[\rho_{Tp}(D_o^2 - D_i^2) + C_A\rho_{flp}D_o^2]\,\mathrm{d}s \tag{28}$$

and

$$\mathrm{d}\bar{m} = \tfrac{1}{4}\pi[\rho_T(x)(D_o^2 - D_i^2) + C_A\rho_{fl}(x)D_o^2]\,\mathrm{d}x. \tag{29}$$

To satisfy the continuity equation for an incremental mass $\mathrm{d}\bar{m}$, equate equations (28) and (29)

$$\tfrac{1}{4}\pi\rho_{Tp}(D_o^2 - D_i^2)\,\mathrm{d}s = \tfrac{1}{4}\pi\rho_T(x)(D_o^2 - D_i^2)\,\mathrm{d}x, \tag{30}$$

and to maintain continuity for the added mass term:

$$\tfrac{1}{4}\pi C_A\rho_{flp}D_o^2\,\mathrm{d}s = \tfrac{1}{4}\pi C_A\rho_{fl}(x)D_o^2\,\mathrm{d}x. \tag{31}$$

Substituting equation (16) into the above equations results in the following relationships between the densities for the perturbed and present Cartesian configurations:

$$\rho_T(x) = \rho_{Tp}\sqrt{1 + v_x(x, t)^2} = \rho_{Tp}\Gamma \tag{32}$$

and

$$\rho_{fl}(x) = \rho_{flp}\sqrt{1 + v_x(x, t)^2} = \rho_{flp}\Gamma, \tag{33}$$

where

$$\Gamma \equiv \sqrt{1 + v_x(x, t)^2} \tag{34}$$

and corresponds to the change of a variable due to a projection onto the x-axis. Substituting equations (32) and (33) into equation (29) yields the differential mass expression where all parameters within the square brackets are assumed constant:

$$\mathrm{d}\bar{m} = \tfrac{1}{4}\pi[\rho_{Tp}(D_o^2 - D_i^2) + C_A\rho_{flp}D_o^2]\Gamma\,\mathrm{d}x. \tag{35}$$

The area moment of inertia for the tendon's cross-section is

$$I(s) = \frac{1}{64}\pi(D_o^4 - D_i^4), \tag{36}$$

and its mass moment of inertia for a thin hollow disk is

$$\begin{aligned} \mathrm{d}J &= \frac{\mathrm{d}\bar{m}I(s)}{A(s)} \\ &= \frac{1}{64}\pi[\rho_T(D_o^2 - D_i^2) + C_A\rho_{fl}D_o^2](D_o^2 + D_i^2)\Gamma\,\mathrm{d}x. \end{aligned} \tag{37}$$

The kinetic energy due to the tendon's linear and angular velocities may be represented by

$$E_k = \int_{s=0}^{s=\ell} \tfrac{1}{2}\,\mathrm{d}\bar{m}[u_t(x,t)^2 + v_t(x,t)^2] + \int_{s=0}^{s=\ell} \tfrac{1}{2}\,\mathrm{d}J\theta_t(x,t)^2. \tag{38}$$

Substituting equations (16), (22) and (37) into equation (38) with the velocities in the x-direction, $u_t(x,t)$, and the y-direction, $v_t(x,t)$, results in the kinetic energy expressed in the present Cartesian frame,

$$\begin{aligned} E_k = \int_{x=0}^{x=L} \Bigg\{ &\frac{1}{8}\pi[\rho_{Tp}(D_o^2 - D_i^2) + C_A\rho_{flp}D_o^2]\Gamma \\ &\times [u_t(x,t)^2 + v_t(x,t)^2] + \frac{1}{128}\pi[\rho_T(D_o^2 - D_i^2) + C_A\rho_{fl}D_o^2] \\ &\times (D_o^2 + D_i^2)\Gamma\theta_t(x,t)\Bigg\}\,\mathrm{d}x, \end{aligned} \tag{39}$$

where the angular velocity, $\theta_t(x,t)$, is found from the geometry:

$$\tan\theta(x,t) = \frac{\mathrm{d}v(x,t)}{\mathrm{d}x}. \tag{40}$$

Differentiating the above equation with respect to time yields

$$[1 + (\tan\theta(x,t))^2]\theta_t(x,t) = v_{xt}(x,t). \tag{41}$$

Substituting equation (40) into equation (41) and rearranging terms results in

$$\theta_t(x,t) = \frac{v_{xt}(x,t)}{\Gamma^2}. \tag{42}$$

In the derivation of the strain energy, $v_x(x,t)^2$ is on the order of $u_x(x,t)$, and $u_x(x,t) \ll 1$, therefore $\Gamma \approx 1$.

5.3. POTENTIAL ENERGY DUE TO GRAVITY AND BUOYANCY

In this section, the potential energy is developed. The tendon's mass and its buoyancy are the two terms of the potential energy. In much of the analytical work

derived by prior researchers, these terms are neglected, in effect it assumes that the tendon is neutrally buoyant. In an actual TLP, the tension contribution from the tendon must be considered. If the tendon does not have sufficient buoyancy, the TLP's payload will have to be reduced or the hull's buoyancy must be increased.

The potential energy due to gravity and buoyancy is expressed as

$$E_p = -\int_{x=0}^{x=L} F_{gb} u \, \mathrm{d}x, \tag{43}$$

where F_{gb} is the force due to gravity and buoyancy of the tendon, and u is the vertical displacement.

The gravitational force is due to the tendon's mass, and its buoyancy is due to the displaced volume of seawater. This yields

$$F_{gb} = -\tfrac{1}{4}\rho_T(x)\pi(D_o^2 - D_i^2)(\ell - s)g + \tfrac{1}{4}\rho_{fl}(x)\pi D_o^2(\ell - s)g, \tag{44}$$

where the first term is due to gravity and the second to buoyancy. The factor $(\ell - s)$ accounts for the length of tendon above position s. Previously, the following relationships were developed:

$$\rho_T(x) = \rho_{Tp}\Gamma, \qquad \rho_{fl}(x) = \rho_{flp}\Gamma. \tag{45, 46}$$

Substituting the above equations into equation (43) results in the expression for the potential energy:

$$E_p = -\int_{x=0}^{x=L} \{\tfrac{1}{4}\pi\{-\rho_{Tp}(D_o^2 - D_i^2) + \rho_{flp}D_o^2\} \cdot (\ell - s) \cdot g\Gamma u\} \, \mathrm{d}x. \tag{47}$$

5.4. ASSEMBLY OF TERMS

Substituting equations (14), (16), (15), (39) and (47) into equation (6) yields the Lagrangian which is substituted to $\mathscr{L}$ to obtain the equations of motion and boundary conditions.

6. TENDON WITH HULL

The tendon has been derived as an elastic element. It is coupled to the hull of the TLP which may be represented as a rigid body. The equation of motion for the hull, which is an ordinary differential equation, will first be presented along with its forces that contribute to the boundary conditions of the tendon. This is the pitch response of the hull. Next, a numerical approach to estimating the magnitude of the tendon projection L, will be discussed. This is useful when assumptions such as small angle are not appropriate. The equations of motion for the transverse and longitudinal vibration of the tendon are presented. Finally, the mixed formulation equation of motion and boundary conditions for the coupled tendon will be presented. This partial differential equation describes the surge response at all points along the tendon. The response at the tendon's top boundary also corresponds to the surge response of the hull.

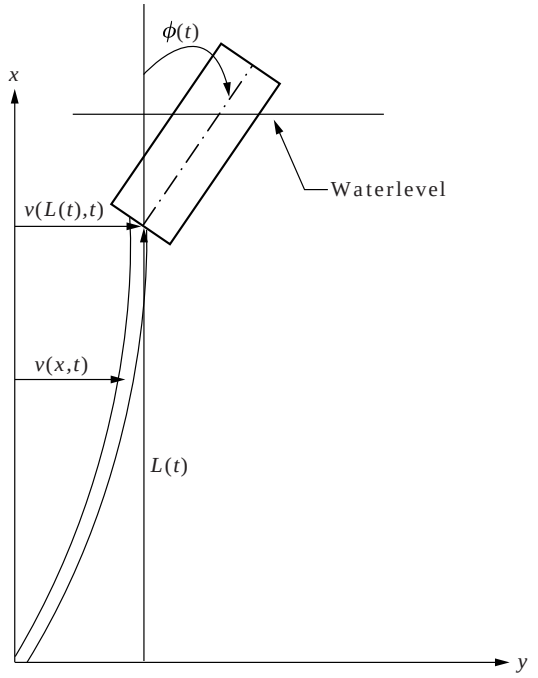

Figure 4. Model of tendon pinned to hull and seafloor.

In Figure 4, the bottom beam represents the tendon with a horizontal displacement of $v(x, t)$. The top mass represents the entire hulland its payload. It is modelled as a rigid body and rotates about the hinge connecting it to the tendon with an angle $\phi(t)$.

6.1. EQUATION OF MOTION FOR HULL PINNED TO TENDON

The equation of motion for the rigid hull is developed in this subsection. First the equations for the hull's kinematics are presented. This is followed with the derivation of the center of buoyancy. This position must be re-evaluated at each instant in time and has generally been neglected in the analytical equations of prior researchers. The kinetics are then derived resulting in the hull's equation of motion and its contribution to the forces on the tendon.

6.1.1. *Kinematics*

The center of mass in the equation below is assumed at the hull's geometric center. As previously discussed, it may be calculated at any position. This is accomplished by simply replacing $L_H/2$ with the appropriate location. The displacement vector from the origin to the hull's center of mass, $\tilde{r}(t)$, is written as

$$\tilde{r}(t) = \left[L(t) + \frac{L_H}{2} \cos \phi \right] \hat{\imath} + \left[v(L(t), t) + \frac{L_H}{2} \sin \phi \right] \hat{\jmath}. \tag{48}$$

The velocity and the acceleration of the hull are

$$\tilde{\dot{r}}(t) = \left[\dot{L}(t) - \frac{L_H}{2}\phi_t \sin\phi\right]\hat{\imath} + \left[\dot{v}(L(t), t) + \frac{L_H}{2}\phi_t \cos\phi\right]\hat{\jmath} \tag{49}$$

and

$$\tilde{\ddot{r}}(t) = \left[\ddot{L}(t) - \frac{L_H}{2}\phi_{tt} \sin\phi - \frac{L_H}{2}\phi_t^2 \cos\phi\right]\hat{\imath}$$

$$+ \left[\ddot{v}(L(t), t) + \frac{L_H}{2}\phi_{tt} \cos\phi - \frac{L_H}{2}\phi_t^2 \sin\phi\right]\hat{\jmath}. \tag{50}$$

For the derivation of the center of buoyancy, the following assumptions are utilized: only planar motion is considered, the hull is a rigid body, the hull's columns always pierce the water surface, and the water level is assumed constant and horizontal across the hull's column at a given instant of time.

The centroid for the submerged volume is derived as

$$\bar{x}' = \frac{\sum \bar{x}_i'}{\sum V_{HS}}$$

$$= \frac{D_H^2}{32L_{HS}(y, t)} \tan^2\phi + \frac{L_{HS}(y, t)}{2} \tag{51}$$

and

$$\bar{y}' = \frac{\sum \bar{y}_i'}{\sum V_{HS}} = \frac{D_H^2 \tan\phi}{16L_{HS}(t)}. \tag{52}$$

Finally, this results in the moment arm, ℓ_b, between the hull's buoyancy forces and the hull pivot in the inertial co-ordinate system of

$$\ell_b = \frac{D_H^2 \tan\phi}{16L_{HS}(y, t)} \cos\phi + \left(\frac{D_H^2 \tan^2\phi}{32L_{HS}(y, t)} + \frac{L_{HS}(y, t)}{2}\right) \sin\phi$$

$$= \left[\frac{D_H^2}{32L_{HS}(y, t)} (2 + \tan^2\phi) + \frac{L_{HS}(y, t)}{2}\right] \sin\phi. \tag{53}$$

6.1.2. *Kinetics*

The kinetics for the hull are now developed in order to derive the hull's equation of motion. The inertia, weight and buoyancy of the hull are also forces on the tendon. Additional buoyancy will increase the tension in the tendon, effectively

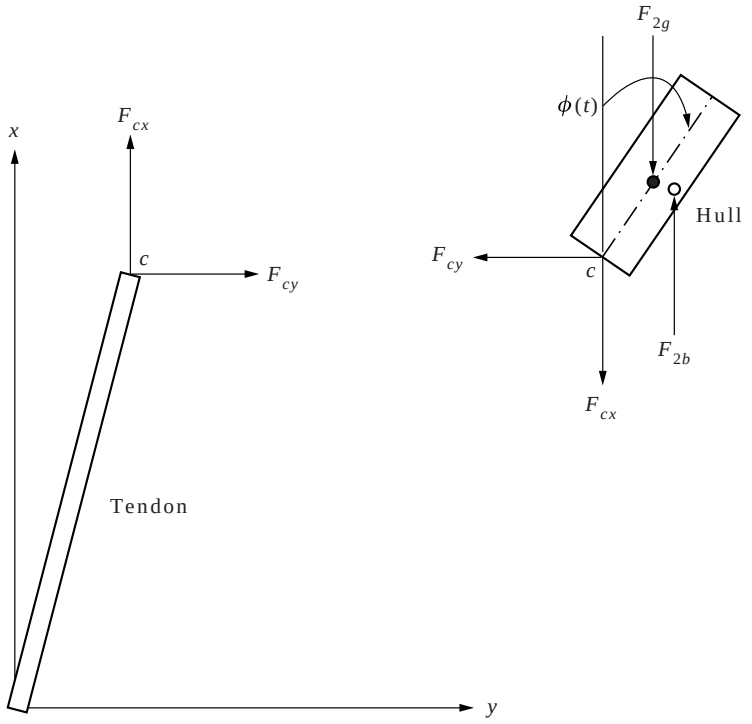

Figure 5. Free body diagram of the hull (waves, current and wind forces not shown).

stiffening the system; see Figure 5. Performing a force balance on the hull and utilizing equation (50) yields:

The sum of the vertical forces, where the terms represent the hull's weight, buoyancy and reaction force equated to the hull's mass (including added mass) multiplied by its vertical acceleration,

$$\sum F_x = F_{2b} - F_{2g} - F_{cx} = \bar{M}\left[\ddot{L}(t) - \frac{L_H}{2}\phi_{tt}\sin\phi - \frac{L_H}{2}\phi_t^2\cos\phi\right]. \tag{54}$$

The sum of the horizontal forces, where the reaction force is equated to the hull's mass (including added mass) multiplied by its horizontal acceleration,

$$\sum F_y = -F_{cy} = \bar{M}\left[\ddot{v}(L(t), t) + \frac{L_H}{2}\phi_{tt}\cos\phi - \frac{L_H}{2}\phi_t^2\sin\phi\right]. \tag{55}$$

The sum of the moments, where the terms represent the hull's weight multiplied by its constant moment arm, its buoyancy multiplied by its variable moment arm, and the moment created by the acceleration of the hull's mass (including

added mass). This is equated to the hull's mass moment of inertia multiplied with its angular acceleration,

$$\sum M_c = F_{2g}\frac{L_H}{2}\sin\phi - F_{2b}\ell_b - \bar{M}\left[\ddot{v}(L(t),t) + \frac{L_H}{2}\phi_{tt}\cos\phi - \frac{L_H}{2}\phi_t^2\sin\phi\right]\frac{L_H}{2}\cos\phi + \bar{M}\left[\ddot{L}(t) - \frac{L_H}{2}\phi_{tt}\sin\phi - \frac{L_H}{2}\phi_t^2\cos\phi\right]\frac{L_H}{2}\sin\phi = J_{cm}\phi_{tt}, \tag{56}$$

where ℓ_b is the moment arm between the buoyancy force and the pivot. The buoyancy and gravitational forces are

$$F_{2b} = \rho_{fl}gV_{HS}(y,t), \qquad F_{2g} = Mg, \tag{57, 58}$$

and F_{cx} and F_{cy} are the vertical and horizonatal reaction forces at the hinge (point c) respectively.

The relationship between the mass moment of inertia for the hull about its center of mass and the pivot is

$$J_H = J_{cm} + \bar{M}\left(\frac{L_H}{2}\right)^2. \tag{59}$$

Substituting equations (53), (57), (58) and (59) into equations (54), (55) and (56) yields the following equations for the reaction forces and the equation of motion of the hull in terms of generalized co-ordinate ϕ:

$$F_{cx} = -\bar{M}\left[\ddot{L}(t) - \frac{L_H}{2}\phi_{tt}\sin\phi - \frac{L_H}{2}\phi_t^2\cos\phi\right] + \rho_{fl}gV_{HS}(y,t) - Mg, \tag{60}$$

$$F_{cy} = -\bar{M}\left[\ddot{v}(L(t),t) + \frac{L_H}{2}\phi_{tt}\cos\phi - \frac{L_H}{2}\phi_t^2\sin\phi\right], \tag{61}$$

and

$$J_H\phi_{tt} - \tfrac{1}{2}MgL_H\sin\phi + \rho_{fl}gV_{HS}(y,t)\left[\frac{D_H^2}{32L_{HS}(t)}(2+\tan^2\phi) + \frac{L_{HS}(y,t)}{2}\right]\sin\phi + \bar{M}\frac{L_H}{2}[\ddot{v}(L(t),t)\cos\phi - \ddot{L}(t)\sin\phi] = Q^{\phi}, \tag{62}$$

where the submerged hull length is

$$L_{HS}(y, t) = \frac{d + \eta(y, t) - L(t)}{\cos \phi}, \tag{63}$$

and Q^{ϕ} is the generalized force associated with the generalized co-ordinate ϕ.

The tension due to the hull equals F_{cx}, where the hull's inertia is $\bar{M}\ddot{L}_x(t)$, the weight of the hull is Mg and its buoyancy is $\rho_{fl} g V_{HS}(y, t)$. The volume of the submerged portion of the hull, $V_{HS}(y, t)$, varies with the displacement of the hull and time. If the hull is assumed to pivot about its attachment to the tendon then, for a constant cross-sectional area, the submerged volume is

$$V_{HS}(y, t) = \pi \frac{D_H^2}{4} \frac{d + \eta(y, t) - L(t)}{\cos \phi}. \tag{64}$$

We see that $R_3^V(t) = F_{cx} + F_{Hfl}^x$, $R_3^H(t) = F_{cy}$ and $Q = -F_{Hfl}^y$ result in the generalized force

$$\hat{Q}^y = \left[-\bar{M}\left[\ddot{L}(t) - \frac{L_H}{2} \phi_{tt} \sin \phi - \frac{L_H}{2} \phi_t^2 \cos \phi \right] \right.$$

$$\left. + \rho_{fl} g \left(\pi \frac{D_H^2 d + \eta(y, t) - L(t)}{\cos \phi} \right) - Mg + F_{Hfl}^x \right]$$

$$\cdot \left[-\frac{3}{2} v_x + \frac{1}{2} v_x|_{x=0} \right]. \tag{65}$$

6.2. EQUATIONS OF MOTION FOR A TENDON WITH A PINNED HULL

In this section, the equation of motion for the tendon, which includes the effects due to its coupling with the hull, is presented. This partial differential equation describes the surge response at all points along the tendon. The response at the tendon's top boundary also corresponds to the surge response of the hull.

The following equations of motion represent the pitch response of the hull, the transverse response of the hull and the tendon and the longitudinal response of the tendon. A binomial expansion was performed on the equations below with respect to v_x, v_{xx}, v_{xxx} and v_{xxxx}, and terms above third order were discarded. In addition, the vertical velocity is assumed small as compared to the horizontal velocity, $u_t \ll v_t$. This expansion was implemented with MAPLE [16].

Equation of motion for the pitch response of the hull:

$$J_{cm}\phi_{tt} - \tfrac{1}{2}MgL_H \sin\phi + \rho_{fl}gV_{HS}(y,t)\left[\frac{D_H^2}{32L_{HS}(t)}(2+\tan^2\phi) + \frac{L_{HS}(y,t)}{2}\right]\sin\phi - \bar{M}\frac{L_H}{2}\left[\ddot{v}(L(t),t)\cos\phi + \frac{L_H}{2}\phi_{tt}\right] = Q_{fl}^{\phi}. \tag{66}$$

Equation of motion for the transverse response of the hull and tendon:

$$-EIv_{xxxx} - \bar{\hat{m}}w_{tt} + \frac{\partial P}{\partial x}v_x + Jv_{xxtt} + Pv_{xx} - \frac{\rho_{fl}g\pi D_H^2}{8\cos\phi}(vv_x^2 + v^2v_{xx}) = \hat{Q}^y. \tag{67}$$

Equation of motion for the longitudinal response of the tendon:

$$\frac{\partial P}{\partial x} - \hat{R}^V = mu_{tt}, \tag{68}$$

where P is the tension in the tendon and $\hat{R}^V$ represents the vertical forces per unit length on the tendon. This is due to the tendon's and hull's weight and buoyancy. The tension is also related to the strain by

$$P = EAe_{xx} = EA\left[\frac{\partial u}{\partial x} - \frac{1}{2}\left(\frac{\partial v}{\partial x}\right)^2\right]. \tag{69}$$

Solving this above expression for displacement u, results in an "Integrability Condition". Details on the "Integrability Condition" are found in Bottega [17, 18].

If the vertical acceleration is assumed negligible as compared to the horizontal acceleration, $u_{tt} \ll v_{tt}$, or equivalently the longitudinal response may be negligible as compared to the transverse response, equation (68) becomes

$$\frac{\partial P}{\partial x} - \hat{R}^V = 0. \tag{70}$$

Solving for the tension in the tendon yields

$$P = (\rho_{fl}A_o - \hat{m})g(L-x) + (\rho_{fl}V_{HS} - M)g. \tag{71}$$

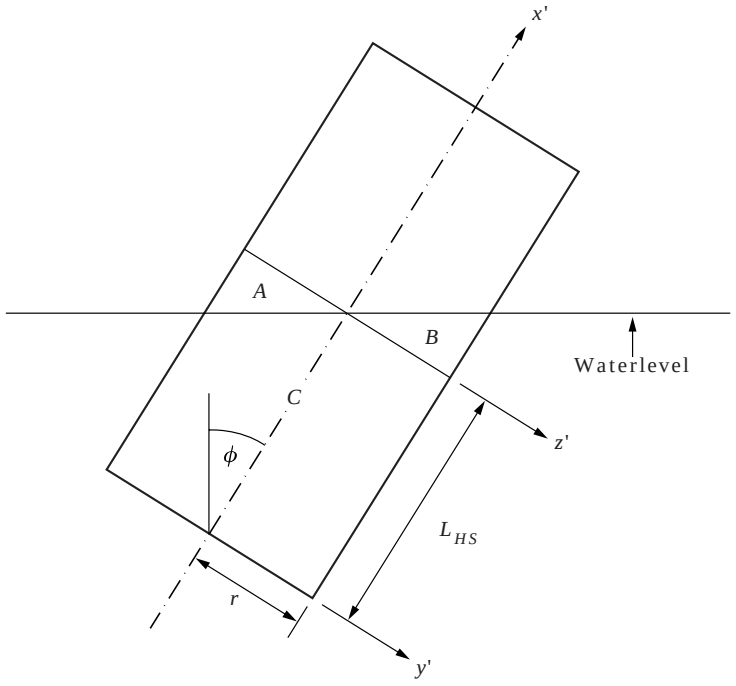

Figure 6. Side view of cylindrical hull for center of buoyancy calculations.

Substituting equation (71) into equation (67) results in a mixed formulation, as described in Bottega [17, 18], for the surge response of the tendon and hull:

$$
\begin{aligned}
&-EIv_{xxxx} - \bar{\hat{m}}v_{tt} \\
&\quad + \left[-(\rho_{fl}A_o - \hat{m})g + \frac{\rho_{fl}g\pi D_H^2}{8\cos\phi}\, vv_{xx} \right] v_x \\
&\quad + Jv_{xxtt} + [(\rho_{fl}A_o - \hat{m})g(L-x) + \rho_{fl}V_{HS} - Mg]v_{xx} \\
&\quad - \frac{\rho_{fl}g\pi D_H^2}{8\cos\phi}\,(vv_x^2 + v^2 v_{xx}) \\
&= \hat{Q}_{fl}^{y}. \qquad (72)
\end{aligned}
$$

The two boundary conditions are

$$
\begin{aligned}
&EIv_{xxx} + \left[-\rho_{fl}V_{HS}g + Mg + \rho_{fl}g\pi\,\frac{D_H^2}{16\cos\phi}\, v^2 \right] v_x \\
&\quad + \frac{1}{2}(\rho_{fl}V_{HS}g - Mg)v \\
&\quad - \bar{M}\left[\ddot{v}(L(t), t) + \frac{L_H}{2}\,\phi_{tt}\cos\phi - \frac{L_H}{2}\,\phi_t^2 \sin\phi \right]\Bigg|_{x=0}^{x=L} + F_{Hfl}^{y} \\
&= 0 \qquad (73)
\end{aligned}
$$

or $\delta v = 0$, which physically prescribes zero transverse displacement and

$$-EIv_{xx} - M_{ft}|_{x=0}^{x=L} = 0 \tag{74}$$

or $\delta v_x = 0$, which physically prescribes vanishing slope.

The forces due to wind, wave and current forces will be included in Q_{ft}^{ϕ}, $\hat{Q}_{ft}^{y}$, F_{Hft}^{x}, F_{Hft}^{y} and M_{ft} which represent the generalized moment on the hull about the revolute joint between the hull and tendon, the generalized force on the tendon, the horizontal and vertical forces due to the fluid forces on the hull and the moment at the ends of the tendon, respectively.

6.2.1. *Normalized equations of motion*

It may be desirable to normalize the equations of motion to distinguish the important terms from those that may be neglected for a particular system. All spatial co-ordinates are normalized with respect to the tendon length ℓ. Temporal co-ordinates are normalized with respect to a time τ, which may be specified as the period corresponding to the first natural frequency of the system. This leads to the relationships

$$\acute{t} = \frac{t}{\tau}, \qquad \acute{x} = \frac{x}{\ell}, \qquad \acute{v} = \frac{v}{\ell}, \qquad \acute{u} = \frac{u}{\ell}. \tag{75–78}$$

The normalized pitch response of the hull from equation (66) is

$$\phi_{\acute{t}\acute{t}} + \beth_1 \sin\phi - \beth_2 \acute{v}_{\acute{t}\acute{t}}(L, t)\cos\phi - \beth_3 \phi_{\acute{t}\acute{t}} = \acute{Q}_{ft}^{\phi}, \tag{79}$$

where the non-dimensional parameters $\beth_1$, $\beth_2$, $\beth_3$ and $\acute{Q}_{ft}^{\phi}$ are

$$\beth_1 = \frac{\tau^2}{J_{cm}}\left[-\frac{1}{2}MgL_H + \rho_{ft}gV_{HS}\frac{D_H^2}{32L_{HS}}(2+\tan^2\phi) + \rho_{ft}gV_{HS}\frac{L_{HS}}{2}\right], \tag{80}$$

$$\beth_2 = \bar{M}\frac{L_H}{2}\frac{\ell}{J_{cm}}, \qquad \beth_3 = \bar{M}\frac{L_H^2}{4}\frac{1}{J_{cm}} \tag{81, 82}$$

and

$$\acute{Q}_{ft}^{\phi} = \frac{\tau^2}{J_{cm}}Q_{ft}^{\phi}.$$

The normalized mixed formulation for surge response of the hull and tendon from equation (72) is

$$\begin{aligned} &-\acute{v}_{\acute{t}\acute{t}} - \beth_4 \acute{v}_{\acute{x}\acute{x}\acute{x}\acute{x}} - \beth_5 \acute{v}_{\acute{x}\acute{x}} + \beth_6 \acute{v}\acute{v}_{\acute{x}}\acute{v}_{\acute{x}\acute{x}} \\ &\quad + \beth_7 v_{xxtt} + \beth_8 \acute{v}_{\acute{x}\acute{x}} - \beth_9 \acute{v}\acute{v}_{\acute{x}}^2 - \beth_{10}\acute{v}^2\acute{v}_{\acute{x}\acute{x}} \\ &= \acute{Q}_{ft}^{y}, \end{aligned} \tag{83}$$

where the non-dimensional parameters $\beth_4$, $\beth_5$, $\beth_6$, $\beth_7$, $\beth_8$, $\beth_9$, $\beth_{10}$ and $\acute{Q}_{ft}^{y}$ are

$$\beth_4 = \frac{EI\tau^2}{\bar{\bar{m}}\ell^4}, \qquad \beth_5 = (\rho_{ft}A_o - \hat{m})g\frac{\tau^2}{\bar{\bar{m}}\ell}, \tag{84, 85}$$

$$\beth_6 = \frac{\rho_{fl} g \pi D_H^2}{8 \cos \phi} \frac{\tau^2}{\bar{\bar{m}} \ell}, \qquad \beth_7 = J \frac{1}{\bar{\bar{m}} \ell^2}, \tag{86, 87}$$

$$\beth_8 = [(\rho_{fl} A_o - \hat{m}) g (L - \dot{x}\ell) + (\rho_{fl} V_{HS} - M) g] \frac{\tau^2}{\bar{\bar{m}} \ell^2}, \tag{88}$$

$$\beth_9 = \frac{\rho_{fl} g \pi D_H^2}{8 \cos \phi} \frac{\tau^2}{\bar{\bar{m}}}, \qquad \beth_{10} = \frac{\rho_{fl} g \pi D_H^2}{8 \cos \phi} \frac{\tau^2}{\bar{\bar{m}}} \tag{89, 90}$$

and

$$\acute{Q}_{fl}^{y} = \frac{\tau^2}{\bar{\bar{m}} \ell} Q_{fl}^{y}. \tag{91}$$

Terms such as $\acute{v}_{\dot{x}\dot{x}\dot{x}\dot{x}}$ may be neglected when the tendon length is very large, as is the case for many tension leg platforms, if the area moment of inertia, I, is moderate. Although general statements cannot be made about the importance of each term, it may be possible to estimate the significance of each term for a specific physical model. In addition, coefficients such as $\beth_4$, which is the normalized bending stiffness, aid in the evaluation of the response in that the importance of the parameters may be seen.

7. WAVE KINEMATICS

In the analysis presented in this paper, linear wave theory is applied [15]. While linear wave theory appears to be an excellent approximation for the forces on the tendon, on the hull, however, non-linear effects may be of importance. The variable wetting of the hull's columns may lead to such higher order effects as ringing [19, 20, 21].

7.1. STOCHASTIC WAVE KINEMATICS

The random wave height power spectrum is transformed into a time history using the method by Borgman [22]. The wave surface profile is given by

$$\eta(v, t) = \frac{H}{2} \cos (kv - \omega t + \varepsilon), \tag{92}$$

where H is the wave height and ϵ the phase. A sample plot of a random wave surface is shown in Figure 7. The Pierson–Moskowitz wave energy spectrum for the significant wave height H_s (see Figure 8) is of the form

$$S_\eta(\omega) = \frac{A_0}{\omega^5} \mathrm{e}^{-B/\omega^4}, \tag{93}$$

where the constants A_0 and B are defined as

$$A_0 = 0{\cdot}0081 g^2, \qquad B = \frac{3{\cdot}11}{H_s^2}. \tag{94, 95}$$

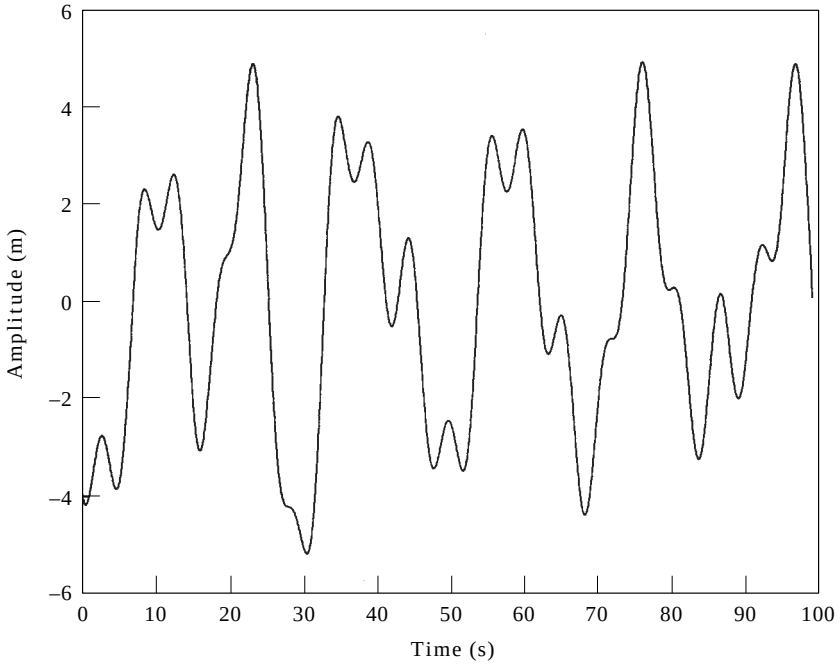

Figure 7. Sample random wave.

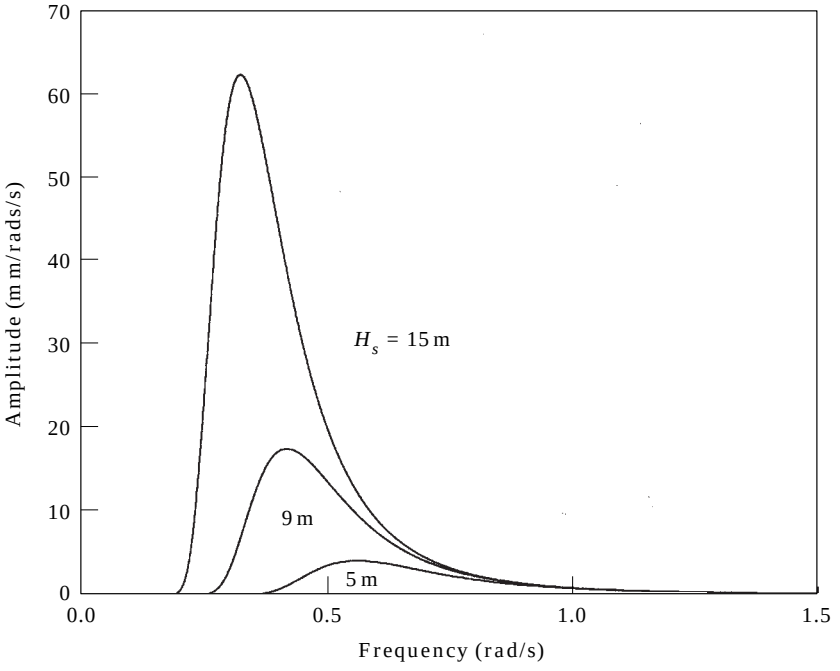

Figure 8. Pierson–Moskowitz spectrum for a significant wave heights of 5, 9 and 15 m.

The wave elevation is approximated as

$$\bar{\eta}(v, t) = \sqrt{\frac{A_0}{4BN}} \sum_{n=1}^{B} \cos(k_n v - \omega_n t + \varepsilon_n), \tag{96}$$

where the partition frequencies ω_n are

$$\omega_n = \left[\frac{B}{\ln(N/n) + B/F^4}\right]^{1/4}, \qquad n = 1, 2, \ldots, N, \tag{97}$$

and the relationship between the wave numbers, k_n, and the frequencies, ω_n, is defined by

$$\omega_n^2 = g k_n \tanh k_n d. \tag{98}$$

F is the terminal frequency, where the wave energy spectrum is truncated at $S_\eta(F)$. The horizontal wave velocity is

$$u_w = \sum_{n=1}^{N} \sqrt{\frac{A_0}{4BN}}\, \omega_n \frac{\cosh k_n x}{\sinh k_n d} \cos(k_n v - \omega_n t + \varepsilon_n), \tag{99}$$

and the vertical wave velocity is

$$w_w = \sum_{n=1}^{N} \sqrt{\frac{A_0}{4BN}}\, \omega_n \frac{\sinh k_n x}{\sinh k_n d} \sin(k_n v - \omega_n t + \varepsilon_n), \tag{100}$$

8. WIND KINEMATICS

The wind speed, $\bar{u}(h)$, is measured empirically at a reference height h above the water surface. There are several definitions for the wind speed. In the United States, the wind speed is measured for a mile of air to pass a fixed point. The highest value during a year is used. The wind velocity at a height z above the water surface is [15]

$$\bar{u}(z) = \left(\frac{z}{h}\right)^{1/n} \bar{u}(h), \tag{101}$$

where $n = 7$ to 8 is used for sustained winds over the open sea, $n = 12$ to 13 for gusts and $n = 7/3$ for rough coastal areas. The wind-stress currents are the result of sustained winds along the water surface.

9. CURRENT KINEMATICS

Ocean current is due to tidal and wind-stress currents and its speed, u_c, may be represented by [15]

$$u_c = \left(\frac{x}{d}\right)^{1/7} u_t(0) + \left(\frac{x}{d}\right) u_w(0), \tag{102}$$

where the values of the maximum current at the water surface for the tidal current, $u_t(0)$, and wind-stress current, $u_w(0)$, are found empirically. Tidal currents are due to the vertical rise and fall of tides and may be as high as 10 knots. The wind-stress currents are the result of sustained winds along the water surface.

10. FORCES

Morison's equation [23] is generally applied to slender offshore structures. For a cylindrical element, the equation for the force per unit length normal to the cylinder is

$$F_{fl} = C_D \rho \frac{D}{2} |V_{fl}^n - V_T^n|(V_{fl}^n - V_T^n) + C_M \rho \pi \frac{D^2}{4} \dot{V}_{fl}^n, \tag{103}$$

where the viscous, frictional drag coefficient C_D and the inertia coefficient C_M are functions of the Reynolds number, the wave characteristics, the cylinder diameter and its roughness. The first term of equation (103) is the drag force, which is the force per unit length required to hold the cylinder in place subject to a stream of relative velocity $(V_{fl}^n - V_T^n)$. The second term is the force per unit length required to hold the cylinder in place subject to a constant free stream acceleration of $\dot{V}_{fl}^n$. The acceleration of the cylinder $\dot{V}_T^n$ was already accounted for in the added mass term.

An alternative form of equation (103) expresses the forces in its components in the inertial frame [24] and may be expressed as

$$\mathbf{F}_{fl} = C_D \rho \frac{D}{2} |\mathbf{l} \times \mathbf{V}_{rel} \times \mathbf{l}|(\mathbf{l} \times \mathbf{V}_{rel} \times \mathbf{l}) + C_M \rho \pi \frac{D^2}{4} (\mathbf{l} \times \dot{\mathbf{V}}_{fl} \times \mathbf{l}), \tag{104}$$

where a unit vector $\mathbf{l}$ along the length of the cylinder expressed in the inertial frame is

$$\mathbf{l} = \cos \alpha \mathbf{i} + \sin \alpha \mathbf{j}. \tag{105}$$

The angle, α, lies between the cylinder and the x-axis, the relative velocity vector is

$$\mathbf{V}_{rel} = \begin{Bmatrix} V_{fl}^x - V_T^x \\ V_{fl}^y - V_T^y \end{Bmatrix}, \tag{106}$$

the fluid acceleration vector is

$$\dot{\mathbf{V}}_{fl} = \begin{Bmatrix} \dot{V}_{fl}^x \\ \dot{V}_{fl}^y \end{Bmatrix}. \tag{107}$$

and the fluid force vector in the inertial frame is

$$\mathbf{F}_{fl} = \begin{Bmatrix} F_{fl}^x \\ F_{fl}^y \end{Bmatrix}. \tag{108}$$

The triple products $(\mathbf{l} \times \dot{\mathbf{V}}_{fl} \times \mathbf{l})$ and $(\mathbf{l} \times \mathbf{V}_{rel} \times \mathbf{l})$ are the fluid acceleration and relative velocities normal to the cylinder expressed in the inertial frame, respectively.

For the fluid forces on the hull, θ is replaced with generalized co-ordinate ϕ. The motion of the tendon is described with the generalized co-ordinate v. Therefore, the following geometrical relationships hold:

$$\sin\theta = \frac{v_x}{\sqrt{1+v_x^2}}, \qquad \cos\theta = \frac{1}{\sqrt{1+v_x^2}}, \qquad \tan\theta = v_x. \tag{109–111}$$

10.1. FLUID FORCES ON THE TENDON

The generalized force per unit length on the tendon will be determined from equation (103), with the relationships for the velocities and accelerations described below.

Morison's equation requires all velocities and acceleration, both of the structure and the fluid, to be normal to the tendon. Therefore, each horizontal velocity and acceleration must be multiplied by $\cos\theta$, equation (110), and all vertical velocities and acceleration by $\sin\theta$, equation (109). The component of the tendon's velocity normal to the tendon may be written as

$$V_T^n = \frac{v_t}{\sqrt{1+v_x^2}}. \tag{112}$$

The velocity of the fluid normal to the tendon due to waves and current is

$$V_{fl}^n = \frac{u_w + u_c - w_w v_x}{\sqrt{1+v_x^2}}. \tag{113}$$

The acceleration of the fluid normal to the tendon due to waves and current is

$$\dot{V}_{fl}^n = \frac{\dot{u}_w - \dot{w}_w v_x}{\sqrt{1+v_x^2}}. \tag{114}$$

This results in the following equation, based on equation (103), for the generalized force per unit length on the tendon:

$$\hat{Q}_{fl}^y = C_D \rho_{fl} \frac{D_o}{2} \left| \frac{u_w + u_c - v_t - w_w v_x}{\sqrt{1+v_x^2}} \right| \left(\frac{u_w + u_c - v_t - w_w v_x}{\sqrt{1+v_x^2}} \right)$$

$$+ C_M \rho_{fl} \pi \frac{D_o^2}{4} \left(\frac{\dot{u}_w - \dot{w}_w v_x}{\sqrt{1+v_x^2}} \right). \tag{115}$$

10.2. FLUID FORCES ON THE HULL

In determining the forces on the hull, the vector form in equation (104) is convenient. The velocity of the hull is required to determine the drag force on the hull, its acceleration was already accounted for in the hull's added mass term, $\bar{M}$.

The displacement vector, $\mathbf{r}_H$, from the origin of the inertial frame to any point along the centerline of the hull is

$$\mathbf{r}_H = [L(t) + x\cos\phi]\mathbf{i} + [v(L(t), t) + x\sin\phi]\mathbf{j}, \tag{116}$$

and its velocity is

$$\dot{\mathbf{r}}_H = [\dot{L}(t) - x\dot{\phi}\sin\phi]\mathbf{i} + [\dot{v}(L(t), t) + x\dot{\phi}\cos\phi]\mathbf{j}, \tag{117}$$

which provides the values of V_T^x and V_T^y required for equation (106). The force per unit length on the hull due to the wave and current forces in the inertial frame is

$$\overline{\mathbf{F}}_{Hfl} = \begin{Bmatrix} \overline{F}_{Hfl}^x \\ \overline{F}_{Hfl}^y \end{Bmatrix}, \tag{118}$$

and the unit vector along the length of the hull is expressed as

$$\mathbf{l} = \cos\phi\,\mathbf{i} + \sin\phi\,\mathbf{j}. \tag{119}$$

This results in a moment about the pivot between the hull and the tendon of

$$Q_{fl}^{\phi} = \int_{x=L}^{x=L+L_{HS}\cos\phi} \{\overline{F}_{Hfl}^y x - \overline{F}_{Hfl}^x x\tan\phi\}\,\mathrm{d}x, \tag{120}$$

where the horizontal and vertical forces per unit length, $\overline{F}_{Hfl}^y$ and $\overline{F}_{Hfl}^x$, are multiplied by their moment arms x and $x\tan\phi$, and integrated over the length of the hull. Similarly, the resultant forces on the tendon in the vertical direction of

$$F_{Hfl}^x = \int_{x=L}^{x=L+L_{HS}\cos\phi} \overline{F}_{Hfl}^x\,\mathrm{d}x, \tag{121}$$

and the horizontal direction of

$$F_{Hfl}^y = \int_{x=L}^{x=L+L_{HS}\cos\phi} \overline{F}_{Hfl}^y\,\mathrm{d}x \tag{122}$$

and found by integrating the forces per unit length over the hull's submerged length from $x = L$ to $x = L + L_{HS}\cos\phi$.

The forces derived in this paper, $\hat{Q}_{fl}^y$, $\hat{Q}_{fl}^{\phi}$, $\hat{F}_{Hfl}^x$ and $\hat{F}_{Hfl}^y$, are then substituted into the equations of motion and corresponding boundary conditions.

10.3. COMPUTATIONAL CHALLENGES

The mathematical model of the TLP consists of a partial differential equation and a set of boundary conditions that describe the motion of the elastic tendon. This is coupled to an ordinary differential equation for the pitch of the rigid hull. The surge response at the top boundary of the tendon is the same as for the hull. Due to the complexities of these equations of motions and the environmental forces, the responses must be solved numerically. These complexities include

recalculating the location of the center of buoyancy and the submerged hull length for each instant in time. Two additional examples are that environmental forces on the hull affect the tension in the tendon, and forces on the tendon affect the set-down of the hull. This set-down in turn changes the hull's buoyancy, and thereby alters the tendon's tension. In this work, the finite difference method is applied spatially, and the resulting ordinary differential equations are evaluated in the time domain.

11. RESPONSE OF THE COUPLED TENDON AND HULL MODEL

This paper presents the response of the coupled tendon and hull model to various ocean wave and current conditions. It addresses the following issues from the literature:

It is important to include wave and current forces on the tendon or solely on the hull? Forces on the tendon have been neglected in much of the literature.
If inclusion of forces on the tendon are important, is it necessary for average or only extral tall TLPs? It has been proposed that the inclusion of environmental forces on the tendon are important for TLPs with lengths on the order of 1500 m.
Does the ratio between the hull's mass and the tendon's mass matter when deciding on how to model the tendon? More detailed treatment of the tendon has been considered of greater value for small hull tendon mass ratios.
What is the effect of selecting a particular estimate of the drag coefficient used in Morison's equation?
How does the selection of the inertia coefficient in Morison's equation affect the response?

In a typical TLP design, the surge, sway and yaw resonance frequencies are below those of the wave frequency range as defined by a power spectrum such as the Pierson–Moskowitz. The heave, pitch and roll resonance frequencies are above this range. The resulting minimal response is a desirable feature of TLPs, and these structures are designed with this in mind. A small vertical displacement greatly

TABLE 1

Properties used for sample velocity profiles

Property	Value
Tendon length	500 m
Water depth	500 m
Water height	15 m
Wave frequency	0·5 rad/s
Wind reference height	10 m
Wind speed at reference height	30 m/s
Exponent n used in wind speed equation	10
Maximum tidal current	2 m/s
Maximum wind-stress current	2 m/s

TABLE 2

TLP properties of quarter ISSC based model

Property	Value
Tendon length	415 m
Tendon outer diameter	0·8 m
Tendon inner diameter	0·3464 m
Tendon density	7800 kg/m^3
Hull length	67·5 m
Hull outer diameter	16·88 m
Hull inner diameter	16·2 m
Hull mass moment of inertia	3·19e6 kg m^2
Hull mass	10·1e6 kg
Modulus of elasticity	204e9 N/m^2
Pontoon height	10·5 m
Pontoon depth	7·5 m
Pontoon length	69·37 m

reduces the cost of equipment used in the drilling for oil and natural gas, and is an important design constraint.

Note: in the response figures presented in this paper, the top graph corresponds to the pitch of the hull. The middle graph corresponds to the surge response of the hull and the top of the tendon. The bottom graph is for the surge response of an illustrative intermediate point along the tendon.

12. RESPONSE OF A 415-m TENDON WITH A 67·5-m HULL

In this section, the response of a model with structural properties listed in Table 2 and fluid properties in Table 3 are presented. These values are based on the International Ship and Offshore Structure Congress (ISSC) TLP model from the ISSC Derived Loads Committee I.2 developed in 1985 and presented in Chatterjee *et al*. [25]. Chatterjee *et al*. studied the response using the finite element method. The ISSC TLP model was developed to allow different researchers to study the same model. It does not correspond to an actual TLP in service to avoid any ties to an individual company.

TABLE 3

Fluid properties of quarter ISSC based model

Property	Value
Mean water level	450 m
Water density	1025 kg/m^3
Significance wave height	9 and 15 m
Drag coefficient	1·0
Inertia coefficient	2·0

The parameters shown in Table 2 are modifications of the ISSC model. The ISSC TLP model has four columns and pontoons and tendons at each corner. Our model is a single tendon–single column idealization, and therefore, the hull's mass was reduced by a factor of four. The hull's volume, which affects the tension in the tendon, is based on the volume of one column (its dimensions are listed as the hull length, hull outer diameter and hull inner diameter), and one rectangular pontoon.

As discussed previously, a single tendon model does not properly capture the pitch response of a hull moored at each corner. The frequency of the pitch response would be higher with the additional tendons, due to the restriction of the pitch of the hull. In order to raise the pitch frequency, the Hull's mass moment of inertia was reduced from 82·37e9 kg m^2 to the values shown in Table 2. The pitch frequency is now within the range of the forcing frequencies of ocean waves. In a traditional TLP design, the pitch frequency will be higher than this range, as will be seen in the case with a 415-m tendon in the next section. The amplitude of the pitch response of the hull is greater for the 415-m tendon model than for the 1415-m tendon model. This is due in part to the 415-m tendon model's natural frequency being in the range of the wave frequencies. The tendon's diameter was not specified in the ISSC model. However, the vertical stiffness of the combined tethers was provided for researchers modelling the tendons as massless springs. Tendon outer and inner diameters were selected based on studying the dimensions of actual TLPs. Structural damping is not included in this analysis, only fluid dissipation due to the drag term in equation (103) is modelled.

12.1. EFFECT OF WAVE AND CURRENT FORCES

The response of the system to stochastic wave forces shows an oscillation about its vertical equilibrium position. This has been well documented in the literature. The response of the tendon is dominated by a rigid body mode. This can be seen by comparing the displacement of the hull with an intermediate point on the tendon. Their peaks are found at approximately the same instants of time.

Current will cause a TLP to oscillate about an offset position rather than its vertical position. This offset in the surge direction has a corresponding setdown, the lowering of the TLP in the heave direction, which increases the buoyancy forces. This results in a higher tension in the tendons than if the tendon and hull were in a vertical position.

12.2. EFFECT OF INCLUSION OF WAVE AND CURRENT FORCES ON THE TENDON

In many of the reviewed papers, tendons were treated as massless springs [26–28]. The response of the TLP, subjected to waves and current along the entire length of the tendon and hull, was compared to a case where these environmental forces are only on the hull (and the top of the tendon since they are connected). In a third case, the forces are on the hull and the top five nodes of the tendon. A plot of the response of all three cases on a single set of graphs shows that inclusion of forces along the entire length of the tendon results in the largest offset as would be expected. This is presented in Figure 9. Forces solely on the hull resulted in the smallest offset. This illustrates the importance of

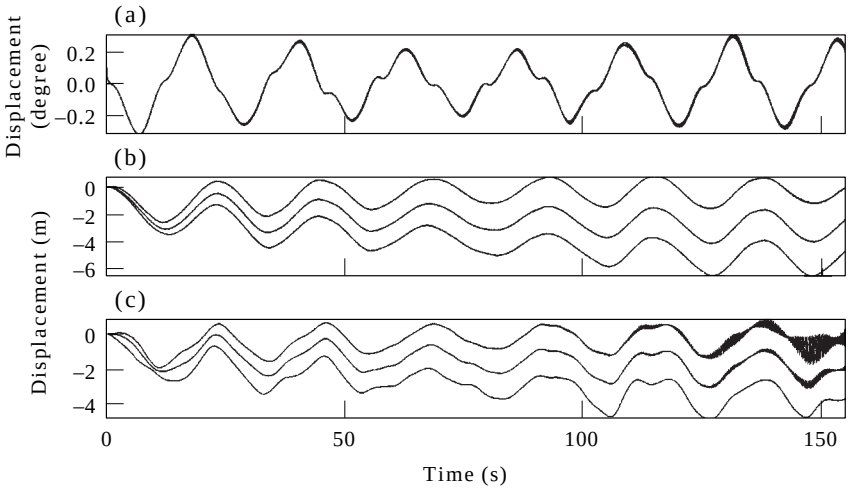

Figure 9. Comparison of three cases: significant wave height of 15 m and current of −10 m/s on a 415-m tendon and a 67·5-m hull: (a) hull pitch, (b) hull surge, (c) tendon surge at 242 m along tendon from its bottom.

including wave and current forces on the tendon. Note that power spectral densities for the responses in this paper may be found in Adrezin [29].

13. RESPONSE OF A 1415-m TENDON WITH A 67·5-m HULL

In the study by Patel and Lynch [30], the hull was modelled as a rigid body with six degrees-of-freedom subject to wave forces. It was coupled to the finite element model of the tendon. This was accomplished by first calculating the response of the hull while assuming a quasi-static tendon stiffness. The hull's displacements were then used in the numerical analysis of the tendon's stiffness. The hull's response was then reevaluated. Only one iteration was performed since the hull's response was predominately due to inertia and the effect of the tendon's stiffness was secondary.

Several perturbations were performed with various physical properties. Patel and Lynch concluded that differences between the quasi-static and dynamic tendon models were minimal except for tendons of lengths on the order of 1500 m or greater. Therefore, the effect of the tendon's dynamics on the hull's response was only significant when the tendons were long, had a large mass per unit length and the hull's displacements were small. The bending stresses in the tendons were also determined to be small. The largest values were found for short tendons with large outer diameters and thin wall thicknesses.

In this section, the TLP of the previous section is reanalyzed with a longer tendon. It is desired to determine the effect of the inclusion of dynamic forces on the tendon. The tendon is now of length 1415 m instead of 415 m. In order to raise the pitch frequency to a realistic level, the hull's mass moment of inertia was reduced from 82·37e9 kg m^2 to the values shown in Table 4. The pitch frequency is now well above the forcing frequencies of ocean waves used in a traditional TLP design. Its structural properties are listed in Table 4 and fluid properties in Table 5.

TABLE 4

Properties of tall TLP model

Property	Value
Tendon length	1415 m
Tendon outer diameter	0·9 m
Tendon inner diameter	0·84 m
Tendon density	7800 kg/m^3
Hull length	67·5 m
Hull outer diameter	16·88 m
Hull inner diameter	16·2 m
Hull mass moment of inertia	3·19e6 kg m^2
Hull mass	10·1e6 kg
Modulus of elasticity	204e9 N/m^2
Pontoon height	10·5 m
Pontoon depth	7·5 m
Pontoon length	69·37 m

13.1. EFFECT OF INCLUSION OF WAVE AND CURRENT FORCES ON THE TENDON

The response of the system to current and stochastic wave forces with a significant wave height of 9 m is compared to a significant wave height of 15 m. This is shown in Figure 11. Both exhibit oscillations about the same offset position due to an equal applied current, but the higher significant wave height led to larger peak amplitudes. Figure 10 shows the profile of the tendon subjected to current and a significant wave height of 9 m.

The response for a TLP subjected to waves with a significant wave height of 15 m and current along the entire length of the tendon and hull. Its power spectrum, exhibits dominant frequencies below 1 Hz, which corresponds to the forcing frequencies of the ocean waves. Dominant frequencies in the pitch response from 4 to 5 Hz may also be seen, corresponding to the overall motion of the hull. This response of the TLP was compared to a case where these environmental forces are only on the hull (and the top of the tendon since they are connected). An additional case, where the forces are on the hull and the top five nodes of the tendon, was also studied. A comparison shows that inclusion of forces along the

TABLE 5

Fluid properties of tall TLP model

Property	Value
Mean water level	1450 m
Water density	1025 kg/m^3
Significance wave height	9 and 15 m
Drag coefficient	1·0
Inertia coefficient	2·0

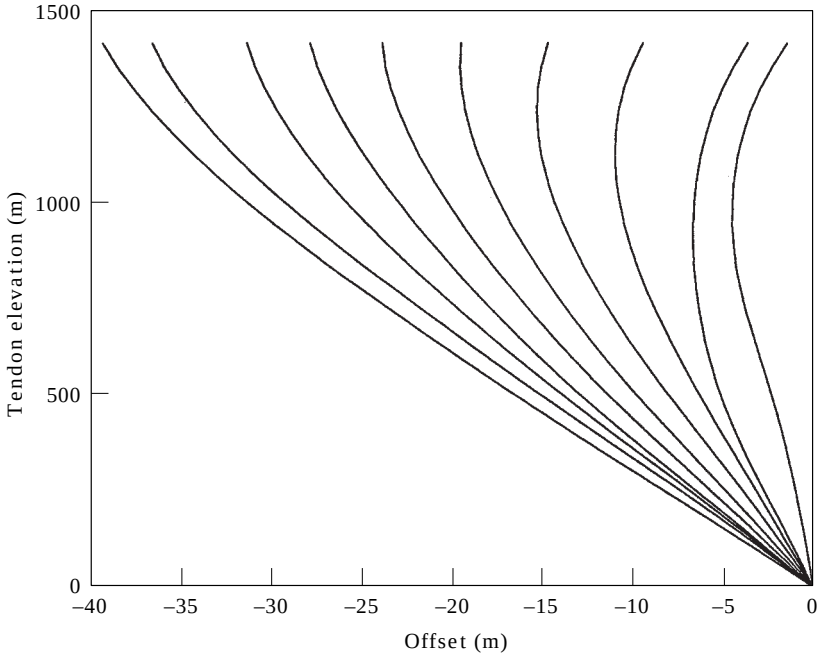

Figure 10. Position of tendon at several time steps.

entire length of the tendon results in the largest offset. Forces solely on the hull resulted in the smallest offset. This illustrates the importance of including wave and current forces on the complete tendon. The power spectral densities were consistent for all three cases.

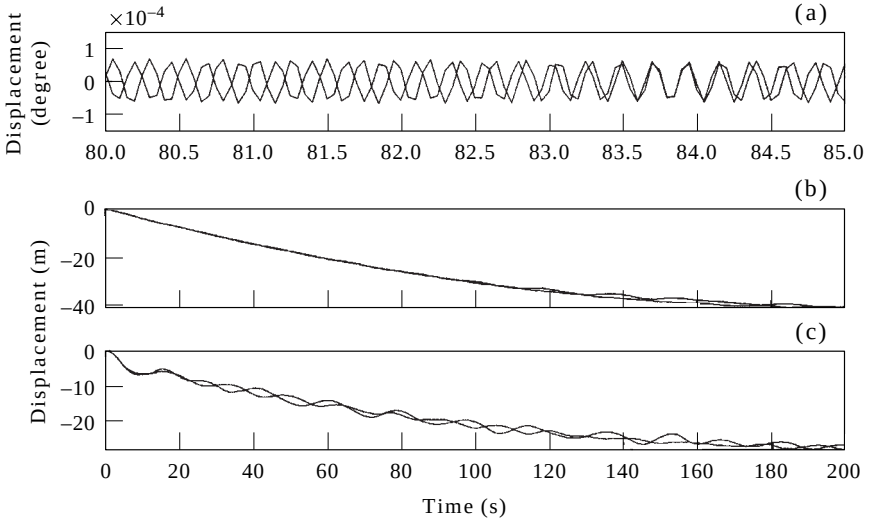

Figure 11. Comparison of a significant wave height of 9 and 15 m, both with a current of -10 m/s on a 1415-m tendon and a 67·5-m hull: (a) hull pitch, (b) hull surge, (c) tendon surge at 825 cm along tendon from its bottom.

14. VARYING THE HULL: TENDON MASS RATIO

The significance of the inclusion of environmental forces on the tendon was explored in a paper by Adrezin and Benaroya [31]. The surge and pitch responses for the hull, and the surge response along the tendon are presented for two cases. Case 1 represents a tendon with a hull mass two orders of magnitude smaller than the tendon's mass. In Case 2, the hull mass is two orders of magnitude greater than the tendon. Inclusion of tendon forces was found to significantly increase the amplitude of the surge response for Case 1 but not for Case 2.

15. MONTE CARLO SIMULATION

As discussed previously, Morison's equation [23] is generally applied to slender offshore structures. For a cylindrical element, the equation for the force per unit length normal to the cylinder is

$$F_{fl} = C_D \rho \frac{D}{2} |V_{fl}^n - V_T^n| (V_{fl}^n - V_T^n) + C_M \rho \pi \frac{D^2}{4} \dot{V}_{fl}^n. \tag{123}$$

The first term of equation (123) is the drag force, which is the force per unit length required to hold the cylinder in place subject to a stream of relative velocity $(V_{fl}^n - V_T^n)$. The second term is the force per unit length required to hold the cylinder in place subject to a constant free stream acceleration of $\dot{V}_{fl}^n$. The acceleration of the cylinder $\dot{V}_{fl}^n$ was already accounted for in the added mass term.

The viscous, frictional drag coefficient C_D and the inertia coefficient C_M are functions of the Reynolds number, the wave characteristics, the cylinder diameter and its roughness. There is no consensus on which values to select for these coefficients [32, 33]. Both tend to be in the range from 0·6 to 2·0. These coefficients may also change over time due to factors such as increasing roughness of the tendons. In this section, a Monte Carlo simulation is performed to account for this spread. A uniform random distribution of coefficients was selected from 0·6 to 2·0 for each coefficient. The results are presented for the TLP with a 1415-m tendon and 67·5-m hull. Its structural properties are listed in Table 4 and fluid properties in Table 5. On a personal computer with a 200-MHz Pentium Pro microprocessor, this series of 40 numerical simulations required about 2 weeks of CPU time.

15.1. DRAG COEFFICIENT

Twenty computer simulations were performed, each with a different drag coefficient in the range from 0·6 to 2·0. The inertia coefficient is held constant at 2·0. The response shows that the offset position and the amplitude are both dependent on the drag coefficient. The surge of the hull is about triple for the case with the maximum displacement as compared to the minimum. Figure 12 shows the mean response banded by the mean plus one standard deviation, and mean minus one standard deviation.

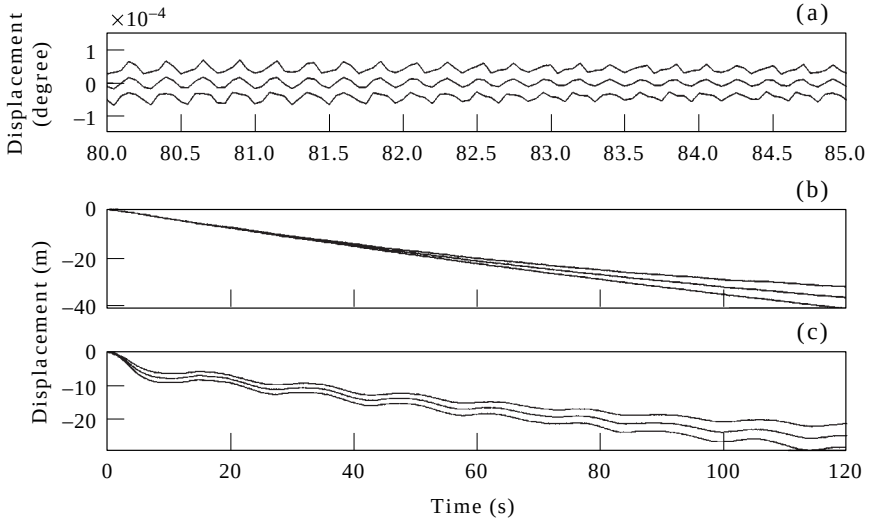

Figure 12. Monte Carlo simulation for drag coefficient +STD/mean/−STD: (a) hull pitch, (b) hull surge, (c) tendon surge at 825 m along tendon from its bottom.

15.2. INERTIA COEFFICIENT

Twenty computer simulations are performed, each with a different inertia coefficient in the range from 0·6 to 2·0. The drag coefficient is held constant at 2·0. The response does not show a significant dependence on the inertia coefficient. A plot of the minimum response subtracted from the maximum response in Figure 13, shows the small differences due to varying the inertia coefficient.

Comparing the drag force with the inertia force term of equation (123), it can be seen that the drag force will be greater for certain conditions. In this Monte

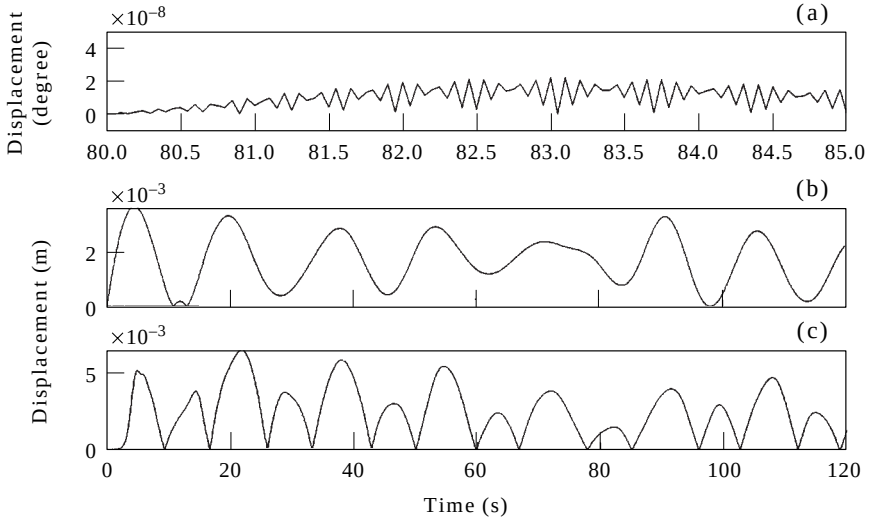

Figure 13. Monte Carlo simulation for inertia coefficient (max − min): (a) hull pitch, (b) hull surge, (c) tendon surge at 825 m along tendon from its bottom.

Carlo simulation, current is included. This has a constant velocity and therefore only contributes to the drag force. A second factor is that the amplitude of the horizontal wave acceleration is equal to the amplitude of the horizontal wave velocity multiplied by the ocean wave frequency. Since these wave frequencies from the Pierson–Moskowitz used in this analysis are less than 1 rad/s, the amplitude of the acceleration is lower than the velocity, resulting in a greater contribution to the drag term. A third effect is due to the outer diameter squared in the inertia term that will result in a smaller inertia effect for the ocean wave forces on the tendon, since its diameter is less than 1 m. Wave forces on the hull however result in a larger contribution from the diameter squared term since the hull diameter is much greater than 1 m.

For certain systems not analyzed here, the inertia term may dominate the drag term. In particular when the hull and tendon diameters are large, the ocean wave frequencies are greater than 1 rad/s and current velocity is low.

16. SUMMARY

A set of non-linear equations of motion for a single-tendon tension leg platform was developed. Many of the simplifying assumptions used by prior researchers have been eliminated. These assumptions are: the tendon may be modelled as a massless spring, ocean forces on the tendon may be neglected, the tendon is neutrally buoyant and therefore its weight and buoyancy may be neglected, the hull and tendon may be treated as uncoupled equations, the change in buoyancy due to hull setdown may be neglected, inculding ocean wave forces with no current, the tendon does not need to be modelled as a beam under time dependent tension, the equation of motions are linear, and the waves are deterministic.

The equations of motion consist of partial differential equations representing the transverse and longitudinal response of the tendon. In addition, a mixed formulation partial differential equation describing the surge response of the hull and tendon, coupled with an ordinary differential equation for the pitch response of the rigid hull is presented. The full derivation with assumptions are presented. These equations may also be applied to other coupled elastic beam/rigid mass problems, such as antennas in space. It is suitable for complex forcing functions and where gravity is present. The response is calculated numerically in the time domain by implementing a finite difference scheme. The equations of motion developed in this paper offer an advantage over those in the literature. Researchers can investigate the terms in these equations to determine which are important for their model.

The response, analyzed for wave and current loading, was presented with a planar motion assumption. The TLP will oscillate about its vertical position due to ocean waves. Current will cause a TLP to oscillate about an offset position rather than its vertical position. This offset in the surge direction has a corresponding setdown, the lowering of the TLP in the heave direction, which increases the buoyancy forces. This results in a higher tension in the tendons than if the tendon and hull were in a vertical position.

Forces on the tendon have been neglected in much of the literature. The responses presented in this work show that the inclusion of forces on the tendon will result in both a greater amplitude and offset position when compared to studies where these forces are neglected. This offset position, which is the surge displacement from the vertical position, is significant in the operation of a TLP. It is necessary to position the hull over the oil wellhead, and therefore surge displacement must be accounted for. This was shown to be important for both a typical height TLP with a 415-m tendon and an extra tall TLP with a 1415-m tendon.

Inclusion of tendon forces on a TLP with a 470-m tendon, where the hull's mass is two orders of magnitude smaller than the tendon's mass, was shown to significantly increase the amplitude of the surge response. This is supported by the literature. However, if the hull mass is two orders of magnitude greater than the tendon, the response is not significantly affected. Note that for the TLP with a 415-m tendon discussed above, its tendon mass was less than one order of magnitude smaller than the hull mass and it showed an increased surge response due to the inclusion of ocean forces on the tendon.

A Monte Carlo simulation was performed on the drag and inertia coefficients in Morison's equation. A uniform random distribution of coefficients was selected from 0·6 to 2·0 for each coefficient. Twenty computer simulations were implemented for each coefficient. The response showed that the offset position and the amplitude are both dependent on the drag coefficient. The surge of the hull shows a maximum offset approximately three times greater for the coefficient that resulted in the maximum displacement than the minimum. The response did not show a significant dependence on the inertia coefficient. The drag term in Morison's equation was dominant over the inertia term due to two main factors. The current was assumed constant and therefore only contributed to the drag force, and the ocean wave frequencies were below 1 rad/s resulting in a smaller contribution to the inertia term. For certain systems not analyzed here, the inertia term may dominate the drag term. In particular when the hull and tendon diameters are large, the ocean wave frequencies are greater than 1 rad/s and current velocity is low.

A significant effort was made in solving these equations of motion numerically. The response is calculated in the time domain by implementing a finite difference scheme. Obtaining solutions that would converge required extensive CPU time. In addition, each parametric study required on the order of weeks of CPU time, limiting the number of parameters that could be varied.

ACKNOWLEDGMENTS

This work was supported by the Office of Naval Research Grant No. N00014-94-1-0753. The first author is grateful for his ONR-sponsored Fellowship, and the second author for additional support. Our program manager, Dr T. Swean, is sincerely thanked for his support as well as his interest in our work. The valuable input from Professors Haim Baruh and William Bottega, and Ms Seon Han and Anette Karlsson of Rutgers University is greatly appreciated.

REFERENCES

1. B. J. Natvig and P. Teigen 1993 *International Journal of Offshore and Polar Engineers* **3**, 241–249. Review of hydrodynamic challenges in TLP design.
2. S. K. Chakrabarti 1987 *Hydrodynamics of Offshore Structures*. Southampton: Computational Mechanics Publications.
3. A. Salpukas 1994 *New York Times*, 7 December, D1, D5. Oil companies drawn to the deep.
4. R. Robison 1995 *Civil Engineering*, 44–47. Bullwinkle's big brother.
5. R. Adrezin, P. Bar-Avi and H. Benaroya 1996 *Journal of Aerospace Engineering* **9**(4), 114–131. Dynamic response of compliant offshore structures—review.
6. P. Bar-Avi and H. Benaroya 1997 *Nonlinear Dynamics of Compliant Offshore Structures*. Lisse, Netherlands: Swets and Zeitlinger Publishers.
7. C. Lanczos 1986 *The Variational Principles of Mechanics*. New York: Dover.
8. H. Baruh (1999) *Analytical Dynamics*. New York: McGraw-Hill.
9. S. K. Clark 1972 *Dynamics of Continuous Elements*. Englewood Cliffs, NJ: Prentice-Hall.
10. A. Bokaian 1994 *Journal of Sound and Vibration* **175**, 607–623. Lock-in prediction of marine risers and tethers.
11. K. Y. R. Billah 1989 *PhD thesis*, *Princeton University*. A study of vortex-induced vibration.
12. P. Bar-Avi and H. Benaroya 1996 *Journal of Sound and Vibration* **198**, 27–50. Planar motion of an articulated tower with an elastic appendage.
13. Y. C. Fung 1994 *A First Course in Continuum Mechanics*. Englewood Cliffs, NJ: Prentice Hall.
14. W. J. Bottega 1986 *Dynamics and Stability of Systems* **1**, 201–215. Dynamics and stability of support excited beam-columns with end mass.
15. J. F. Wilson 1984 *Dynamics of Offshore Structures*. New York: Wiley.
16. Waterloo maple inc.
17. W. J. Bottega 1990 *AIAA Journal* **28**, 2008–2011. Instability of a partially delaminated surface layer of an oscillating cylinder.
18. W. J. Bottega 1994 *International Journal of Solids Structures* **31**, 1891–1909. On circumferential splitting of a laminated cylindrical shell.
19. S. B. Kim, E. J. Powers, R. W. Miksad and F. J. Fischer 1991 *Proceedings of the First International Offshore and Polar Engineering Conference* **1**, 87–92. Quantification of nonlinear energy transfer to sum and difference frequency responses of TLP's.
20. B. J. Natvig and H. Vogel 1991 *Proceedings of the First International Offshore and Polar Engineering Conference* **1,** 93–99. Sum-frequency excitations in TLP design.
21. X. B. Chen, B. Molin and F. Petitjean 1995 *Marine Structures* **8**, 501–524. Numerical evaluations of the springing loads on tension leg platforms.
22. L. E. Borgman 1969 *Journal of the Waterways and Harbors Division* **95**, 557–583. Ocean wave simulation for engineering design.
23. J. R. Morison, M. P. O'Brien, J. W. Johnson and S. A. Schaaf 1950 *Petroleum Transactions*, *AIME* **189**, 149–154. The force exerted by surface waves on piles.
24. S. Gran 1992 *A Course in Ocean Engineering*. Amsterdam: Elsevier.
25. P. C. Chatterjee, P. K. Das and D. Faulkner 1997 *Ocean Engineering* **24**, 313–334. A hydro-structural analysis program for TLPs.
26. A. Kareem 1995 *Journal of Structural Engineering* **111**, 37–55. Wind-induced response analysis of tension leg platforms.
27. W. S. Park, C. B. Yun and B. K. Yu 1991 *Proceedings of the First International Offshore and Polar Engineering Conference* **1**, 108–116. Reliability analysis of tension leg platforms by domain crossing approach.
28. B. J. Natvig 1994 *Proceedings of the Fourth International Offshore and Polar Engineering Conference* **1**, 40–51. A proposed ringing analysis model for higher order tether response.

29. R. S. ADREZIN 1997 *PhD thesis*, *Rutgers*. The nonlinear stochastic dynamics of tension leg platforms.
30. M. H. PATEL and E. J. LYNCH 1983 *Engineering Structures* **5**, 299–308. Coupled dynamics of tensioned buoyant platforms and mooring tethers.
31. R. ADREZIN and H. BENAROYA (1998) *Journal of Probabilistic Engineering Mechanics* **14**(1/2), 3–17. Response of a tension leg platform to stochastic wave forces.
32. B. B. MEKHA, C. P. JOHNSON and J. M. ROESSET 1994 *Proceedings of the Fourth International Offshore and Polar Engineering Conference* **1**, 105–115. Effects of different wave free surface approximations on the response of a TLP in deep water.
33. X. SONG and A. KAREEM 1994 *OMAE* **1**, 123–134. Combined system analysis of tension leg platforms: a parallel computational scheme.

APPENDIX: NOMENCLATURE

d	mean water level (water depth)
ℓ	length of tendon
$\hat{m}$	tendon mass per unit length
$\bar{\hat{m}}$	tendon mass per unit length (including added mass)
$v(x, t)$	horizontal displacement of a point x on the tendon
A	tendon cross-sectional area of hollow tendon
A_o	tendon cross-sectional area of solid tendon
D_H	outer diameter of the cylindrical hull
D_{Hi}	inner diameter of cylindrical hull
D_i	tendon inner diameter
D_o	tendon outer diameter
I	area moment of inertia of the tendon
J	mass moment of inertia of a thin hollow disk of tendon (including added mass)
J_{cm}	mass moment of inertia of a hull about its center of mass (including added mass)
J_H	mass moment of inertia of hull about the pivot connecting it to the tendon (including added mass)
$\mathscr{L}$	Lagrangian
L	projected length of tendon onto the x-axis
L_H	length of hull
$L_{HS}(v, t)$	length of submerged portion of the hull measured along its centerline
M	hull mass
$\bar{M}$	hull mass (including added mass)
$M_3(t)$	generic moment on the hull about the pivot connecting it to the tendon
P	tension in the tendon
$\hat{Q}^y$	generalized force per unit length in the y-direction
Q^ϕ	generalized force associated with the generalized co-ordinate ϕ
$R(x)$	radius of curvature
$\hat{R}_1^V(t)$	generic vertical force per unit length
$\hat{R}_1^H(t)$	generic horizontal force per unit length
$\hat{R}_2^V(x, t)$	generic vertical force per unit length
$\hat{R}_2^H(x, t)$	generic horizontal force per unit length
$\hat{R}_3^V(x, v, v_x, v_{xx}, v_{xxx}, t)$	generic vertical force per unit length
$R_3^H(t)$	generic horizontal force on the hull passing through the pivot connecting it to the tendon
T	kinetic energy

V	potential energy
$V_{HS}(v, t)$	volume of the submerged portion of the hull
W	work
$\eta(y, t)$	wave height elevation
ρ_T	tendon density in reference configuration
$\rho_{Tp}(s)$	tendon density in perturbed configuration
ρ_{fl}	water density in reference configuration
$\rho_{flp}(s)$	water density in perturbed configuration